Materials Research Bulletin 91 (2017) 173–178

Contents lists available at ScienceDirect

Materials Research Bulletin

journal homepage: www.elsevier.com/locate/matresbu

Silver nanoparticles for detection of methimazole by surface-enhanced Raman spectroscopy

Tawfik A. Saleh*[,1], Mutasem M. Al-Shalalfeh, Abdulaziz A. Al-Saadi

Department of Chemistry, King Fahd University of Petroleum & Minerals, Dhahran 31261, Saudi Arabia

ARTICLE INFO

Article history:
Received 11 January 2017
Received in revised form 15 March 2017
Accepted 21 March 2017
Available online 23 March 2017

Keywords:
Nanoparticles
Methimazole
SERS
DFT calculation
Interface

ABSTRACT

An efficient method was developed for quantitative detection of methimazole using surface enhanced Raman spectroscopy (SERS). Silver nanoparticles (AgNPs) were prepared by a reduction method and designed as SERS substrates for the detection of methimazole, which is of medicinal importance. The morphology and the structure of the nanoparticles were characterized using a transmission electron microscope, a UV–vis spectroscopy, a Fourier transformed infrared spectroscopy and a Raman spectroscopy. The average size of the AgNPs was 60 nm. The UV–vis spectrum showed a characteristic maximum absorbance at around 420 nm for AgNPs. The adsorption behavior of methimazole on the AgNPs substrates was investigated by SERS and density functional theory (DFT) calculations. SERS experimental and theoretical results imply that a chemical interaction is considered between the NPs and methimazole. SERS experiments indicated an enhancement in the bands, which was utilized to develop a linear correlation between the methimazole concentrations and SERS signal intensity.

1. Introduction

Methimazole (MTZ), known as 1-methylimidazole-2-thiol, is used in thyroid hormone biosynthesis by preventing the organification of iodide in the thyroid [1]. MTZ as an antithyroid drug is used for the treatment of hyperthyroidism, and in Graves' disease [2]. MTZ is one of the azole derivatives that extensively used in the field of inhibition of metals from corrosion [3], Fig. 1. Due to its presence in a wide range of pharmaceutical formulations and body fluids, the determination of MTZ is a significant area of interest. MTZ has been investigated by various methods including; electrochemical techniques, high-performance liquid chromatography, gas chromatography, fluorescence probe method, infrared and Raman spectroscopies [4,5]. However, these techniques required additional derivatization procedure and more time-consuming [6].

Surface Enhanced Raman Scattering (SERS), an advanced method of Raman technique, has become a center of interest for molecular characterization. SERS is a promising alternative method for the analysis of the biological and pharmaceutical compounds, due to its high-sensitivity, and non-destructive nature [7]. Spectral intensities in SERS are enhanced by a high factor, for example, 10^8–10^{10} can be obtained for target molecules adsorbed on the substrate surface compared to traditional Raman spectroscopy [8]. This enhancement is arising from the two main factors, electromagnetic and chemical charge transfer enhancements [9–11].

Several studies were reported for the investigation of pharmaceutical compounds in aqueous solution, using metal nanoparticles [12–14]. Due to attractive physicochemical properties, surface plasmon resonance, silver, and gold nanoparticles have been used as substrates for the structural investigation of some drugs such as mefenorex, pentylenetetrazole, L-amphetamine, pemoline, MTZ and cyclodextrin [15,16]. The molecular properties of the MTZ have been reported using FTIR, Raman, and SERS [17,18]. However, up to the best of our knowledge, there is no studies reported a quantitative method for the determination of MTZ by SERS.

The aim and motivation of this work was to develop a sensitive method without the need for sample preparation for the detection of methimazole in medical formulations using SERS with substrates of silver nanoparticles (AgNPs). DFT calculations were carried out for the bands assignment. The developed method was evaluated for the determination of MTZ in pharmaceutical forms.

* Corresponding author.
E-mail addresses: tawfik@kfupm.edu.sa, tawfikas@hotmail.com (T.A. Saleh).
[1] Home Page: http://faculty.kfupm.edu.sa/CHEM/tawfik/.

http://dx.doi.org/10.1016/j.materresbull.2017.03.041
0025-5408/

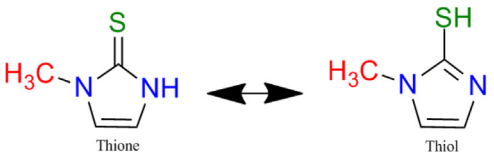

Fig. 1. Structures of Methimazole Forms.

2. Experimental

2.1. Chemicals and materials

Methimazole, 1-Methyl-2-imidazolethiol, analytical standard, ≥99% purity, the CAS number 60560, were purchased from Sigma-Aldrich. Trisodium citrate dihydrate ($C_6H_5Na_3O_7{\cdot}2H_2O$, 98%) **(cat number is S-279, product number 78479**) was purchased from Fisher Scientific Company in U.S.A. Silver nitrate ($AgNO_3$, 99.8%), product number 30087, was purchased from BDH-Chemicals Ltd Poole England. Potassium bromide (KBr, ≥99%) was purchased from Sigma-Aldrich and used for making KBr pellets with silver nanoparticles for obtaining IR spectrum. Solutions were prepared with ultrapure water obtained from a water purification system (Ultra Clear™ Lab Water Systems, Siemens Water Technologies USA).

2.2. Synthesis

AgNPs were prepared by the following procedure. First, a solution of 0.1 M silver nitrate was prepared by dissolving $AgNO_3$ in 250 ml of deionized water, followed by heating the solution at 90 °C. Then, 10 ml of 0.5% solution of trisodium citrate dihydrate was added at a rate 1 drop/sec to the solution under stirring. After adding 5 ml, the solution color turned yellow. The solution was kept under boiling for one hour, the color of the solution changed to greenish yellow.

2.3. Characterization

The nanomaterials were characterized by various methods including; TEM technique to determine the particle size, morphology, and particle distributions of nanomaterials. The TEM images were taken using the JEM −2100F Field Emission Electron Microscope, JEOL- USA, at 200 kV acceleration voltage. The UV–vis spectra of the NPs were recorded on a genesis 10S UV–vis spectrophotometer (Thermo Scientific), using standard quartz cuvette at room temperature between 200 and 700 nm ranges. The colloid samples were prepared by dilution the stock solution 4x with distilled water.

2.4. Surface-enhanced Raman spectroscopy (SERS)

The SERS spectra of MTZ were obtained by using Raman spectroscopy system Lab Ram HP Evolution Raman spectrometer equipped with an internal He-Ne 17 mW laser at a 633 nm excitation wavelength. The laser was used on 10% power at the sample. SERS samples were prepared by using a 3: 1 volume ratio of the MTZ solutions to the colloid. A 10x objective was used for focusing the laser beam to the solution. The data acquisition time was 30 s with one accumulation for collection each SERS spectra. A cuvette with dimensions of 1 cm radius, 2 cm height was used as a sample cell for the Raman spectra. The SERS spectra were obtained in the range from 400 to 2000 cm^{-1}. The solid sample was prepared by adding a small amount of the MTZ solid on a glass slide for obtaining the spectrum using laser λ 633 nm, the acquisition time of 30 sec and objective 10x.

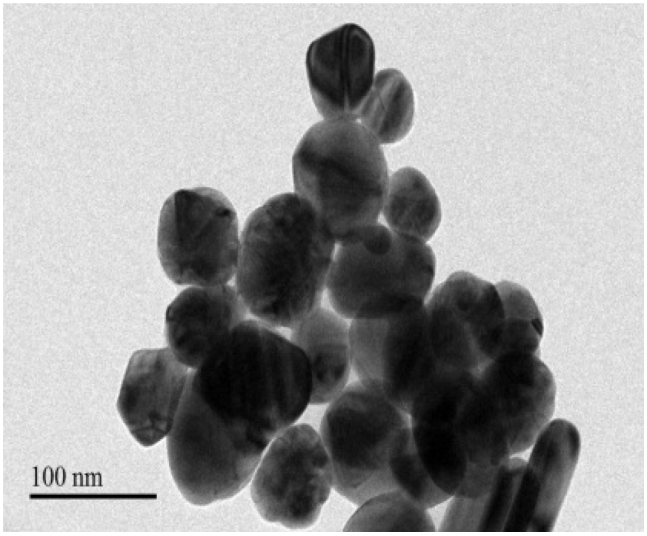

Fig. 2. The typical TEM images of AgNPs.

2.5. Computational details

The ab initio and DFT calculations were employed to assign the bands used for the detection of MTZ compound. The GAUSSIAN 09 program running on an IBM RS/6000 model S85 Unix server was used to carry out the DFT/B3LYP calculations. The 6–311++G (d, p) triple basis set was employed to optimize the structure of the compound. The Gauss −View program was used to collect the vibrational assignment, and Raman line activity of MTZ compound.

3. Results and dissections

3.1. Characterization

Fig. 2 shows the TEM image of AgNPs, which indicates uniform shape and well-dispersed particles with the average size of about ~60 nm as estimated by TEM scale. The Ultraviolet −visible (UV–vis) absorption spectrum AgNPs are shown in Fig. 3. The absorption characteristic maximum of AgNPs showed surface plasmon resonance band at 421 nm. The Raman spectra of the nanoparticles were given in Fig. 4. In the case of silver, no clear Raman bands were observed in the 200 cm^{-1} to 3000 cm^{-1} range of the spectra. However, it can be observed the spectra show a weak broadband 1380–1420 cm^{-1} and a very small peak at 926 cm^{-1} in silver.

3.2. Vibrational assignments

3.2.1. Vibrational assignment theoretically by DFT

The calculated wavenumbers were scaled using the scaling factor 0.961 for frequency region ≥2000 cm^{-1}, and scaling factor 0.985 for frequency region >2000 cm^{-1} [19–21]. The calculated CH stretching vibrational modes for MTZ is assigned at 3162, 3142, 3022, 2998, 2929 cm^{-1} which is corresponding to ν (C7-H), ν (C6-H), ν (C5-H11), ν (C5-H12), and ν (C5-H13). The NH stretching vibrational mode can be assigned at 3531 cm^{-1} in theoretical spectra. The band at 1588 cm^{-1} is corresponding to C=C stretching vibration mode. The C—S stretching vibrational modes were predicted to have four vibrational frequencies, at 1473, 1459, 1415 and at 1159 cm^{-1}. The peak at 238 cm^{-1} is attributed to C—S wag mode. The N-H in plane bending was assigned at three different frequencies. The NH (CH) mode (out the plane, and in plane) vibration was predicted at three different frequencies, the ring bend (in plane) was predicted three different vibrations, and at one

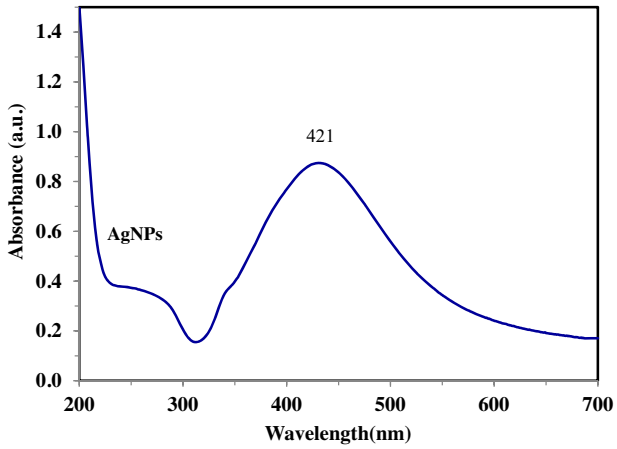

Fig. 3. Absorption spectrum AgNPs, where a.u. stands for arbitrary unit.

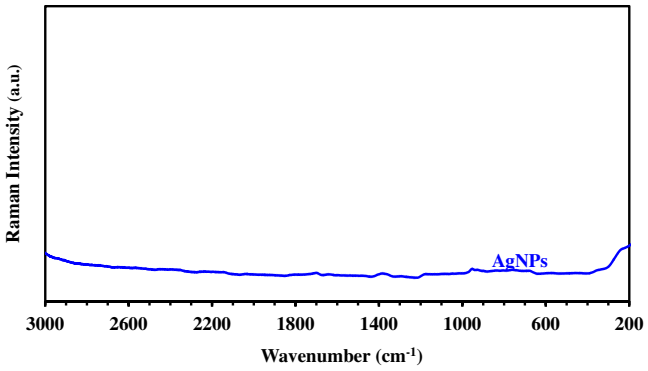

Fig. 4. Raman spectra of AgNPs.

position for ring bend (out plane). The SCN vibration mode was predicted at two different frequencies. These vibrations are in the mix with other vibrational modes, Fig. 5.

3.2.2. Vibrational assignments experimentally

Raman experimental modes, shown in Fig. 6, are in correlation with the calculated results. For example, the C—H stretching mode for MTZ in this study was predicted theoretically at 3162 cm^{-1}, which is in a very good agreement with the experimentally observed IR bands at 3161 cm^{-1}, and with the Raman peaks at

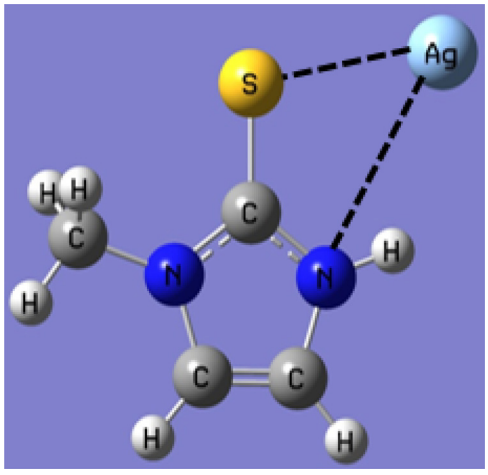

Fig. 5. The optimized structures of the MTZ-silver.

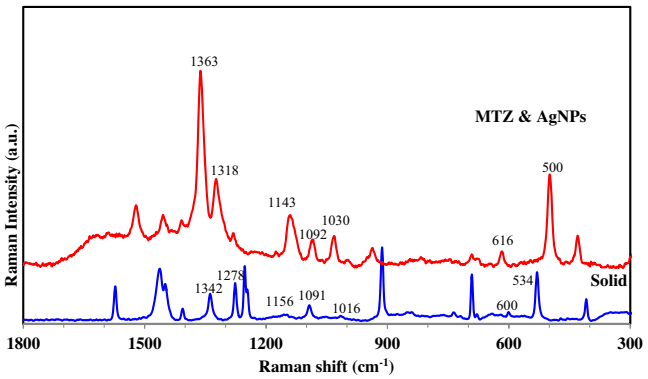

Fig. 6. Raman spectrum of solid MTZ and SERS spectra of 1×10^{-5} M MTZ with AgNPs. Laser λ 633 nm, acquisition time; 30 s, and objective; 10x.

3166 cm^{-1} of a previous study [12,22]. The stretching vibration of S—C at 1415 cm^{-1} in the Raman experimental spectrum, and at 1403 cm^{-1} in the IR experimental spectrum appears at 1410 cm^{-1} in the theoretical spectrum. The C=C stretching vibrational theoretically assigned at 1588 cm^{-1} can be assigned at 1578 cm^{-1} in the IR experimental spectrum, and at 1579 cm^{-1} in the Raman experimental spectrum, which is in a good agreement with the reported IR spectra in the literature [12,15]. The C—N stretching vibrational was predicted at 1315, 1285, 1212, 1159 cm^{-1} in the theoretical spectra, are assigned at 1339, 1274, 1248, 1152 cm^{-1} in the IR experimental spectrum, and were observed at 1342, 1278, 1252, 1156 cm^{-1} in the Raman experimental spectrum, respectively. These are in agreement with the literature [5,22]. The observed N—C—S in- plane bending vibration at 534, and 411 cm^{-1} in the theoretical spectrum appears at (527, and 411) cm^{-1}, and (525, 410) cm^{-1} in the IR and Raman experimental spectrum, respectively. This is in agreement with earlier reported by Chandra and Chowdhury [23].

3.2.3. DFT calculations of MTZ –silver

The obvious difference between the SERS and normal Raman spectra is frequency shifts and changes in the intensity for most of the bands. The silver complex of the MTZ conformers were optimized using the DFT method with B3LYP/GEN basis set. In both cases, the results of the theoretical calculation show the stable structures when the nanoparticles are close and interact with the S, and N atoms, as shown in Fig. 5. A single atom of Ag was used in the DFT calculation because both atoms have larger van der Waals radii than both S and N atoms hence it is easier for one atom of Ag to interact with S and N atoms. However, using a cluster of Ag atoms led to the presence of imaginary frequencies in the calculated spectra, which meant the calculation did not converge and there might be repulsion between the metal atoms. Hence the use of one atom of Ag in the DFT calculation.

The agreement between the solid, SERS of MTZ, and the vibrational frequencies of MTZ-Ag complex are calculated through DFT method. The band at 1315 cm^{-1} is shifted to a higher frequency in the calculated values. In the observed experimental case, the band is shifted from 1342 cm^{-1} to 1363 cm^{-1}. The band at 1285 cm^{-1} is moved to higher wavenumber in the theoretical and is in a very good agreement with the experimental data, which is shifted from 1278 cm^{-1} to 1318 cm^{-1} in the SERS-Ag spectrum.

3.3. SERS results of MTZ on the Ag nanoparticles

The Fig. 6 shows the normal Raman spectrum and SERS spectra of the AgNPs with the 1×10^{-5} M MTZ. The band at 1342 cm^{-1} in

the normal Raman spectrum shifted to 1363 cm^{-1} in the SERS spectrum. This band shows a significant enhancement in SERS spectrum. The bands at 1278, 1156, 1091, 1016, and 600 cm^{-1} in the normal Raman spectrum are shifted to 1318, 1143, 1092, 1030, and 616 cm^{-1}, respectively in the SERS spectrum. These bands are enhanced to higher intensities in SERS spectrum than normal Raman spectrum. The band at 534 cm^{-1} in the normal Raman spectrum is observed at 500 cm^{-1} in the SERS spectrum. This band is attributed to SCN bending and shows a significant enhancement in SERS spectrum.

The enhancement of the intensities of the N—C, S—C, and N—H stretching indicated that the MTZ ring directly interacts with the nanoparticles through the unpaired electron on the N and S atom. According to the SERS electromagnetic enhancement mechanism [24,25], and the metal surface selection rules [26]. The groups are very close to the metal surface with a tilted orientation should be more enhanced than the groups are parallel to the metal surface. This is in agreement with our SERS theoretical calculation conducted in this study. These surface selection rules should apply to adsorption on the nanoparticles with a diameter more than 20 Å. However, less enhancement for the smaller particles is expected [27].

3.3.1. SERS enhancement factor of MTZ

The SERS enhancement factors for the vibrations of MTZ (1×10^{-3} M) the NPs to the corresponding band obtained from 1.0 M saturated solution were calculated using the following equation.

$$EFs = (\delta_{SERS} \times C_{normal})/(\delta_{normal} \times C_{SERS})$$

Where δ and C are the Raman mode intensity and sample concentration, respectively. The EFs for the SERS peaks of MTZ on the NPs are given in Table 1. The EFs is not the same for the different MTZ modes, the maximum enhancement was observed at 1342 cm^{-1}.

3.3.2. Calibration curve and method validation

On the other hand, Fig. 7a shows the concentrations dependent SERS spectra of MTZ obtained by using AgNPs. The SERS intensity increases proportionally with increasing the concentrations of the MTZ solution in the range from 10^{-7}M to 10^{-12}M. The highest enhanced band at 1363 cm^{-1} in SERS spectra was selected for creating a quantitative analysis of MTZ. Fig. 7b shows the calibration curve of MTZ solution with AgNPs. The linear SERS response from 10^{-7} M to 10^{-12} M of MTZ was obtained with a good linear coefficient (R^2) of 0.9989 and relative standard deviation of 1.9%.

The linear equations and correlation coefficients of MTZ with NPs substrates are listed in Table 2. A good linear correlation between the Raman peak intensities and MTZ concentrations were noted with wide linear working range (LWR) for MTZ with both substrates. However, AgNPs showed lower detection limits which were obtained according to the equation:

$$LOD = 3 \times SD + B_{ave}$$

LOD: limit of detection; SD: standard deviation; B_{ave}: average measurement of the blank.

The results obtained by the reported method in this study were compared with some methods reported in the literature in term of calibration range, detection limits, and determination coefficient (R^2). The comparison with other methods for the determination of MTZ is summarized in Table 3. It is clear that the method is comparable to other methods.

3.3.3. Determination of MTZ in real samples

Determination of MTZ in Tablet samples was examined to demonstrate the ability of the SERS method for the determination of MTZ in real samples. The proposed method was applied for the determination of MTZ in the real pharmaceutical samples. For this purpose, tablet samples were obtained. In order to access the matrix effect, the relative recoveries of the method were calculated. The results given in Table 4 indicate that the SERS method retained its efficiency for the determination of MTZ in real samples. It should be mentioned that the Raman modes of MTZ in the pharmaceutical samples can be seen clearly with almost no interference because the additives in the samples are not Raman active within the considered working range between 300 and 1800 cm^{-1}.

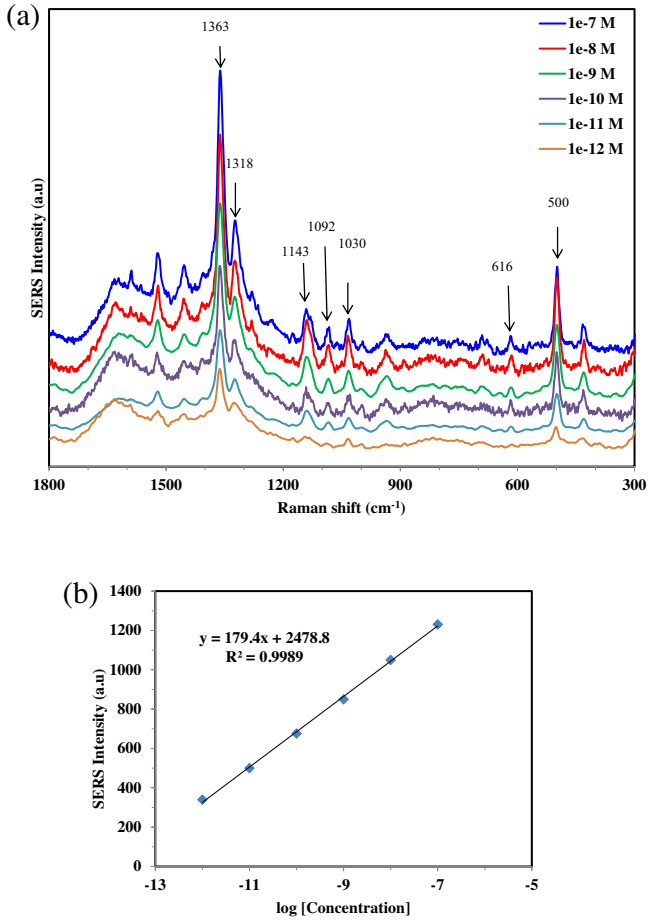

Fig. 7. (a) SERS spectra of MTZ with different concentration using AgNPs, b) calibration curve of the band at 1363 cm^{-1}, using AgNPs. Laser λ = 633 nm, acquisition time; 30 s, and objective; 10x.

Table 1
SERS enhancement factor of MTZ on the NPs.

Substrate	Normal Raman spectra (cm^{-1})	SERS spectra (cm^{-1})	EFs*
AgNPs	1342	1363	9.6×10^4
	1278	1318	2.2×10^4
	1156	1143	4.4×10^4
	1092	1092	2.1×10^4
	1016	1030	3.4×10^4
	600	616	1.4×10^4
	534	500	1.8×10^4

* Average of three measurements.

Table 2
Analytical parameters (features) and regression equation obtained from linear curves for MTZ determination using the SERS.

NPs Type	Raman Peaks	Regression Equation	R^2	Dynamic range	SD	LOD
AgNPs	1363 cm^{-1}	y = 179.4x + 2478.8	0.9989	(10^{-7}–10^{-12})M	1.58	5.01×10^{-14}
	1318 cm^{-1}	y = 74x + 1093.3	0.9964	(10^{-7}–10^{-12}) M	2.74	3.4×10^{-14}
	500 cm^{-1}	y = 74.8x + 1027	0.9812	(10^{-8}–10^{-12}) M	1.82	3.8×10^{-13}

Table 3
Comparison of linear concentration ranges and detection limits with other methods for the determination of MTZ.

Method	Calibration range (M)	Detection limits (M)	R^2	Ref.
SERS	1.0×10^{-12}–1.0×10^{-7}	5.01×10^{-14}	0.9989	Present work
SERS	5.0×10^{-8}–5.5×10^{-7}	7.4×10^{-5}	0.998	[5]
HPLC	0.2×10^{-6}–2.0×10^{-6}	0.18×10^{-6}	0.9975	[31]
Flow-Injection	1.75×10^{-5}–8.75×10^{-4}	8.75×10^{-6}	0.999	[28]
Capillary Electrophoresis	1.0×10^{-7}–2.0×10^{-4}	5.0×10^{-8}	0.9995	[29]
DPV	1.0×10^{-7}–2.0×10^{-5}	2.0×10^{-8}	0.998	[30]
SERS	1.8×10^{-9}–1.3×10^{-6}	8.8×10^{-10}	0.9992	[15]
SWV	6.0×10^{-6}–240×10^{-6}	1.98×10^{-6}	0.9996	[32]

Table 4
Determination of MTZ in pharmaceutical tablets samples (n = 3); Recovered concentrations obtained for MTZ using SERS method with AgNPs and calibration curve at 1363 cm^{-1} (n = 3).

Sample	Expected	Found	Recovery %	Confidence interval	Bias (%)
Tablet 1	5 mg/g	4.87 mg/g	97.4	0.23×10^{-6} M	−2.6
Tablet 2	5 mg/g	4.91 mg/g	98.2	0.23×10^{-6} M	−1.8
Spiked 1	2.5×10^{-6} M	2.51×10^{-6} M	100.3	0.64×10^{-6} M	+0.3
Spiked 2	5.0×10^{-6} M	5.12×10^{-6} M	102.4	0.56×10^{-6} M	+2.4

4. Conclusions

The AgNPs as colloids were prepared by reduction method with about 60 nm particle size. The SERS method was exploited to record the vibrational frequencies of MTZ adsorbed on AgNPs. The optimized conformation and vibrational assignments of MTZ have been carried out using the DFT calculation with B3LYP/6–311++G (d, p) basis set. The vibration assignments and the wavenumber of vibration frequency bands in the theoretical spectra were in agreement with those of the experimental spectra. Most of the bands related to N atom and S atom were apparently enhanced and shifted. These results confirm that MTZ molecules were adsorbed on the silver substrate through probably the lone pair on N and S atoms. The correlation between the MTZ concentration and the SERS signal was linear and of good detection limits.

Acknowledgements

The authors would like to acknowledge the support provided by King Abdulaziz City for Science and Technology (KACST) through project No. A.T.34-8. The authors would like also to acknowledge the support by King Fahd University of Petroleum and Minerals (KFUPM).

Appendix A. Supplementary data

Supplementary data associated with this article can be found, in the online version, at http://dx.doi.org/10.1016/j.materresbull.2017.03.041.

References

[1] A.P. Weetman, A.M. McGregor, Evidence for an effect of antithyroid drugs on the natural history of Graves' disease, Clin. Endocrinol. 21 (1984) 163–172.
[2] B. Georg, R. Dankwart, K. Georg, et al., Is there a methimazole dose effect on remission ratein Graves' disease? Results from a long-termprospective study, Clin. Endocrinol. 49 (1998) 451–457.
[3] R. Subramanian, V. Lakshminarayanan, Effect of adsorption of some azoles on copper passivation in alkaline medium, Corros. Sci. 44 (2002) 535–554.
[4] J.Y. Sun, C.Y. Zheng, X.L. Xiao, L. Niu, T.Y. You, E.K. Wang, Electrochemical detection of methimazole by capillary electrophoresis at a carbon fiber microdisk electrode, Electroanalysis 17 (2005) 1675–1680.
[5] Xue Liao, Yanhua Chen, Meihong Qin, Yang Chen, Hanqi Zhang, Yuan Tian, Au–Ag–Au double shell nanoparticles-based localized surface plasmon resonance and surface-enhanced Raman scattering biosensor for sensitive detection of 2-mercapto-1-methylimidazole, Talanta 117 (2013) 203–208.
[6] D.L. Poster, M.M. Schantz, L.C. Sander, S.A. Wise, Analysis of polycyclic aromatic hydrocarbons (PAHs) in environmental samples: a critical review of gas chromatographic (GC) methods, Anal. Bioanal. Chem. 4 (2006) 859–881.
[7] P. Ma, F. Liang, Y. Sun, Y. Jin, X. ChenY. Wang, Y. Wang, H. Zhang, D. Gao, D. Song, Rapid determination of melamine in milk and milk powder by surface-enhanced Raman spectroscopy and using cyclodextrindecorated silver nanoparticles, Microchim. Acta 180 (2013) 1173–1180.
[8] Pedro H.C. Camargo, Leslie Au, Matthew Rycenga, Weiyang Li, Younan Xia, Measuring the SERS enhancement factors of dimers with different structures constructed from silver nanocubes, Chem. Phys. Lett. 484 (2010) 304–308.
[9] Huanping Yang, Hailong Hu, Zhenhua Ni, et al., Comparison of surface-enhanced Raman scattering on graphene oxide, reduced graphene oxide and graphene surfaces, Carbon 62 (2013) 422–429.
[10] Shuang Lin, Wu-Li-Ji Hasi, Xiang Lin, Si-qin-gao-wa Han, Xiu-Tao Lou, Fang Yang, Dian-Yang Lin, Zhi-Wei Lu, Rapid and sensitive SERS method for determination of Rhodamine B in chili powder with paper-based substrates, Anal. Methods 7 (2015) 5289–5294.
[11] Nandita Biswas, Sudhir Kapoor, Harbir S. Mahal, Tulsi Mukherjee, Adsorption of CGA on colloidal silver particles: DFT and SERS study.Chem, Phys. Lett. 20017 (444) (2016) 338–345.
[12] M.M. Al-Shalalfeh, A.T. Onawole, T.A. Saleh, A.A. Al-Saadi, Spherical silver nanoparticles as substrates in surface-enhanced Raman spectroscopy for enhanced characterization of ketoconazole, Mater. Sci. Eng.: C 76 (2017) 356–364.
[13] T.A. Saleh, M.M. Al-Shalalfeh, A. Onawole, A.A. Al-Saadi, Ultra-trace detection of methimazole by surface-enhanced Raman spectroscopy using gold substrate, Vibrational Spectroscopy (2017). http://dx.doi.org/10.1016/j.vibspec.2017.03.009.
[14] T.A. Saleh, M.M. Al-Shalalfeh, A.A. Al-Saadi, Graphene Dendrimer-stabilized silver nanoparticles for detection of methimazole using Surfaceenhanced Raman scattering with computational assignment, Nature Publishing group, Scientific Reports, 6:32185, (2016) DOI: 10.1038/srep32185.
[15] Pinyi Ma, Fanghui Liang, Qingqing Yang, Ying Sun Di Wang, Xinghua Wang, Dejiang Gao, Daqian Song, Highly sensitive SERS probe for mercury(II) using cyclodextrin-protected silver nanoparticles functionalized with methimazole, Microchim. Acta 181 (2014) 975–998.
[16] A. Ruperez, R. Montes, J.J. Lasema, Identification of stimulant drugs by surface-enhanced Raman spectrometry on colloidal silver, Vib. Spectrosc. 2 (1991) 145–154.

[17] Maurizio Muniz-Miranda, Francesco Muniz-Miranda, Alfonso Pedone, Raman and DFT study of methimazole chemisorbed on gold colloidal nanoparticles, Phys. Chem. Chem. Phys 18 (2016) 5974.
[18] Nandita Biswas, Susy Thomas, Anjana Sarkar, Tulsi Mukherjee, Sudhir Kapoor, Adsorption of methimazole on silver nanoparticles: FTIR, Raman, and surface-enhanced Raman scattering study aided by density functional theory, J. Phys. Chem. C 113 (2009) 7091–7100.
[19] Akl M. Awwad, Nidà M. Salem, Amany O. Abdeen, Biosynthesis of silver nanoparticles using Olea europaea leaves extract and its antibacterial activity, Nanosci. Nanotechnol. 2 (6) (2012) 164–170.
[20] Shoba Narayan, Ashwini Rajagopalan, Jannampalli Shruthi Reddya, Anju Chadha, BSA binding to silica capped gold nanostructures: effect of surface cap and conjugation design on nanostructure–BSA interface, RSC Adv. 4 (2014) 1412–1420.
[21] A.A. Al-Shalalfeh, T.A. Saleh, A.A. Al-Saadi, Silver colloid and film substrates in surface-enhanced Raman scattering for 2-thiouracil detection, RSC Adv. 6 (79) (2016) 75282–75292.
[22] S. Bhandari, M. Deepa, et al., Revelation of graphene-Au for direct write deposition and characterization, Nanoscale Res. Lett. 6 (2011) 424–431.
[23] Subhendu Chandra, Joydeep Chowdhury, Manash Ghosh, G.B. Talapatra, Genesis of enhanced Raman bands in SERS spectra of 2-mercaptoimidazole: FTIR, Raman, DFT, and SERS, J. Phys. Chem. A 116 (2012) 10934–10947.
[24] Adam D. McFarland, Matthew A. Young, Jon A. Dieringer, Richard P. Van Duyne, Wavelength-scanned surface-enhanced Raman excitation spectroscopy, J. Phys. Chem. B 109 (2005) 11279–11285.
[25] N. Félidj, J. Aubard, G. Lévi, J.R. Krenn, et al., Controlling the optical response of regular arrays of gold particles for surface-enhanced Raman scattering, Phys. Rev. B 65 (2002) 1–9.
[26] M. Moskovits, J.S. Suh, Surface selection rules for surface-enhanced Raman spectroscopy, J. Phys. Chem. 88 (1984) 5526–5530.
[27] Robert G. Greenler, D.R. Snider, Donald Witt, R.S. Sorbello, The metal-surface selection rule for infrared spectra of molecules adsorbed on small metal particles, Surf. Sci. 118 (1982) 415–428.
[28] Anastasios Economou, Paraskevas D. Tzanavaras, Maria Notou, Demetrius G. Themelis, Determination of methimazole and carbimazole by flow-injection with chemiluminescence detection based on the inhibition of the Cu(II)-catalysed luminol–hydrogen peroxide reaction, Anal. Chim. Acta 505 (2004) 129–133.
[29] Jinying Sun, Chunying Zheng, Xinli Xiao, Li Niu, Tianyan You, Erkang Wanga, Electrochemical detection of methimazole by capillary electrophoresis at a carbon fiber microdisk electrode, Electroanalysis 17 (2005) 1675–1680.
[30] Wang Yazhen, Electrochemical determination of methimazole based on the acetylene black/chitosan film electrode and its application to rat serum samples, Bioelectrochemistry 81 (2011) 86–90.
[31] Robert Zakrzewski, Determination of methimazole in pharmaceutical preparations using an HPLC method coupled with an iodine-azide post-column reaction, J. Liq. Chromatogr. Relat. Technol. 32 (2009) 383–398.
[32] Leonard Molero, Mario Faundez, María Angélica del Valle, Rodrigo del Río, Francisco Armijo, Electrochemistry of methimazole on fluorine-doped tin oxide electrodes and its square-wave voltammetric determination in pharmaceutical formulations, Electrochim. Acta 88 (2013) 871–876.